PHYSICAL REVIEW LETTERS

Articles published week ending 11 APRIL 2014

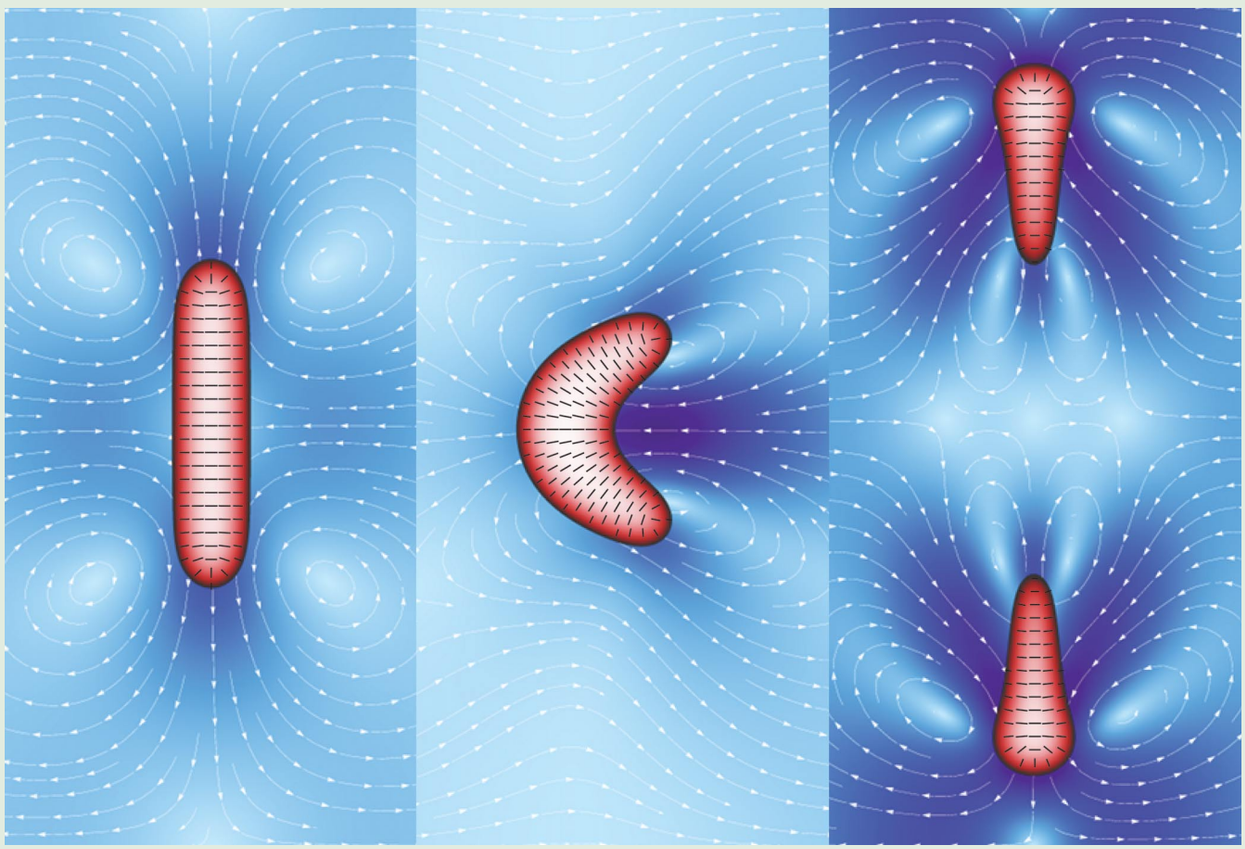

Published by
American Physical Society

APS physics

Volume 112, Number 14

Spontaneous Division and Motility in Active Nematic Droplets

Luca Giomi and Antonio DeSimone
SISSA, International School for Advanced Studies, Via Bonomea 265, 34136 Trieste, Italy
(Received 7 October 2013; revised manuscript received 9 December 2013; published 10 April 2014)

We investigate the mechanics of an active droplet endowed with internal nematic order and surrounded by an isotropic Newtonian fluid. Using numerical simulations we demonstrate that, due to the interplay between the active stresses and the defective geometry of the nematic director, this system exhibits two of the fundamental functions of living cells: spontaneous division and motility, by means of self-generated hydrodynamic flows. These behaviors can be selectively activated by controlling a single physical parameter, namely, an active variant of the capillary number.

DOI: 10.1103/PhysRevLett.112.147802 PACS numbers: 61.30.Jf, 42.70.Df, 87.16.Ka

The goal of understanding the machinery of life has led in recent years to the ambitious idea of constructing synthetic minimal cells: chemical machines capable of reproducing some of the fundamental traits of living cells such as self-maintaining, duplicating, and passing information across generations [1–3]. The first challenge in this program is to identify the crossover region between molecular self-assembly and molecular operation [4], a task that has led to investigate the mechanics of self-dividing lipid vesicles [5,6] and, more recently, the coupling of self-dividing vesicles with self-replicating nucleic acids enclosed in the interior of the vesicle [7,8]. Mass transfer due to hydrodynamic instabilities, such as the Marangoni effect, has been recently invoked as a possible route to motility in prebiotic structures [9].

While a description of the general properties of living matter is beyond the reach of existing theoretical approaches, the paradigm of *active systems* has provided in recent years a promising framework to portray the emergent mechanical behavior of a number of biological and bioinspired materials. Active systems are nonequilibrium assemblies of orientationally ordered self-driven particles. Each active particle is capable of converting stored or ambient energy into systematic movement. The interaction of active particles with each other and with the surrounding medium gives rise to mechanical stresses and highly correlated collective motion over large scales [10–13]. Originally developed for modeling collections of swimming [14] and crawling cells [15], and later extended to the cytoskeleton and its components [10,16,17], the mechanics of active matter has gained increasing attention in the last decade thanks to its successes in the modeling of cellular motility, intracellular movement, and transport [18].

In this Letter we illustrate a remarkable example of cell mimicry in a two-dimensional active droplet endowed with internal nematic order and surrounded by an isotropic Newtonian fluid. Because of the interplay between the active stresses and the geometry of the nematic director, which is constrained by the droplet topology, this system exhibits two of the defining functions of living cells: spontaneous division and motility, by means of self-generated hydrodynamic flows. These behaviors can be selectively activated by controlling a single physical parameter corresponding to an active variant of the capillary number. As in the case of minimal cell models based on oil droplets in water [9,19], the purpose of this work is to explore physical mechanisms leading to cell-like behaviors.

The hydrodynamic equations of an active nematic medium have been proposed based on phenomenological arguments [10,11,20,21], or derived from microscopic models [22–24]. Our system is an incompressible two-phase fluid consisting of a nematic phase embedded in an isotropic phase. The two phases have, for simplicity, the same density ρ, which is then constant throughout the system. We call $\boldsymbol{v}$ the flow velocity and $\boldsymbol{Q}$ the nematic tensor field which, for uniaxial nematics in two dimensions, is given by $Q_{ij} = S(n_i n_j - \delta_{ij}/2)$, where $\boldsymbol{n}$ is the nematic director and $0 \leq S \leq 1$ is the order parameter representing the local extent of nematic order.

In order to implement the mechanism of phase separation we use a diffuse interface method similar to that proposed in Ref. [25] to simulate two-phase flows in complex fluids. In this picture the two phases are described by a phase field $-1 \leq \phi \leq 1$, such that $\phi = -1$ represents the isotropic phase, $\phi = 1$ the nematic phase, and $\phi \approx 0$ the diffuse interface. The effective capillarity of the interface can be described starting from a Ginzburg-Landau energy density of the form

$$f_{\text{cap}} = \frac{1}{2}\kappa\left[|\nabla\phi|^2 + \frac{1}{2\epsilon^2}(\phi^2 - 1)^2\right]. \tag{1}$$

This functional favors the separation of the phases into domains of pure components (i.e., $\phi = \pm 1$). The surface tension Σ of the interface is related to the parameters appearing in Eq. (1) by $\Sigma = \sqrt{8}/3(\kappa/\epsilon)$ [25–27]. The interfacial tension gives rise to a body force of the form

$\boldsymbol{f}_{\rm cap} = -\phi\nabla\mu$ [28], where $\mu = \delta F_{\rm cap}/\delta\phi = -\kappa[\Delta\phi - \phi(\phi^2-1)/\epsilon^2]$ is an effective chemical potential. This force is experienced by the system only along the diffuse interface where μ undergoes an abrupt spatial variation. Furthermore, the incompressibility of the fluid phases implies $d/dt\int dA\phi = 0$ and $\nabla\cdot\boldsymbol{v} = 0$. The hydrodynamic equations for the fields ϕ, $\boldsymbol{Q}$, and the flow velocity $\boldsymbol{v}$ are then given by [11,21]

$$\frac{D\phi}{Dt} = M\kappa\left[\Delta\phi - \frac{\phi(\phi^2-1)}{\epsilon^2} + \xi(\phi)\right], \tag{2a}$$

$$\rho\frac{Dv_i}{Dt} = \eta\Delta v_i - \partial_i p - \phi\partial_i\mu + \partial_j\sigma_{ij}, \tag{2b}$$

$$\frac{DQ_{ij}}{Dt} = \lambda S u_{ij} + Q_{ik}\omega_{kj} - \omega_{ik}Q_{kj} + \gamma^{-1}H_{ij}, \tag{2c}$$

where $D/Dt = \partial_t + \boldsymbol{v}\cdot\nabla$ is the material time derivative, M is a mobility coefficient, η the viscosity (also assumed to be the same in both fluids), and p the pressure. The function ξ is a Lagrange multiplier that guarantees mass conservation:

$$\xi(\phi) = |\phi^2-1|\frac{\int dA\phi(\phi^2-1)}{\int dA|\phi^2-1|}. \tag{3}$$

This form was recently introduced [29] as an alternative to a more classic nonlocal expression [30], and leads to higher accuracy in mass conservation by combining both local and nonlocal terms. In Eq. (2c) $u_{ij} = (\partial_i v_j + \partial_j v_i)/2$ and $\omega_{ij} = (\partial_i v_j - \partial_j v_i)/2$ are the rate of strain and the vorticity tensors representing the coupling between orientational order and flow (with λ the flow alignment parameter [31]). The molecular field H_{ij}, on the other hand, drives the relaxational dynamics of the nematic phase (with γ a rotational viscosity) and can be obtained from the variation of the total free energy of the nematic phase $F_{\rm nem} = \int dA(f_{\rm LdG} + f_{\rm anc})$ as $H_{ij} = -\delta F_{\rm nem}/\delta Q_{ij}$. Here, the Landau–de Gennes free energy density $f_{\rm LdG}$ governs the behavior of the bulk nematic phase:

$$f_{\rm LdG} = \frac{1}{2}K\left[|\nabla\boldsymbol{Q}|^2 + \frac{1}{\delta^2}{\rm tr}\boldsymbol{Q}^2({\rm tr}\boldsymbol{Q}^2 - \phi)\right], \tag{4}$$

where K is an elastic constant (proportional to the classic Frank constant) and the second term in Eq. (4) leads to a second order isotropic-nematic phase transition controlled by the phase-field ϕ. Since ${\rm tr}\boldsymbol{Q}^2 = S^2/2$, Eq. (4) implies that, where $\phi = -1$, $f_{\rm LdG}$ has a minimum for $S = 0$, corresponding to the isotropic phase, and for $\phi = 1$, $f_{\rm LdG}$ is minimized by $S = \sqrt{\phi} = 1$.

The term $f_{\rm anc}$ represents the anchoring energy at the isotropic-nematic interface. Here we use a diffuse version of the Nobili-Durand anchoring energy [32]:

$$f_{\rm anc} = \frac{1}{2}W{\rm tr}(|\nabla\phi|^2\boldsymbol{Q} - \boldsymbol{A})^2, \tag{5}$$

where $A_{ij} = \partial_i\phi\partial_j\phi - |\nabla\phi|^2\delta_{ij}/2$. The effect of $f_{\rm anc}$ is to favor a director field $\boldsymbol{n}$ parallel to $\nabla\phi$ (hence normal to the interface) and the value $S = 1$ for the nematic order parameter.

Finally, the stress tensor $\boldsymbol{\sigma} = \boldsymbol{\sigma}^{\rm r} + \boldsymbol{\sigma}^{\rm a}$ is the sum of the elastic stress due to nematic elasticity, $\sigma^{\rm r}_{ij} = -\lambda S H_{ij} + Q_{ik}H_{kj} - H_{ik}Q_{kj}$ and of an active contribution $\sigma^{\rm a}_{ij} = \alpha Q_{ij}$ that describes contractile ($\alpha > 0$) and extensile ($\alpha < 0$) stresses exerted by the active particles in the direction of the director field.

We have integrated Eqs. (2) numerically in a square $L\times L$ domain with periodic boundary conditions. The initial configuration consists of a circular droplet of radius $R = L/10$, with director field uniformly aligned and the flow velocity identically zero. The integration is performed using a vorticity or stream-function finite difference scheme on a collocated grid of lattice spacing $\Delta x = \Delta y = 0.078$. The time integration was performed via a fourth-order Runge-Kutta method with time step $\Delta t = 10^{-3}$ [11,21]. To make Eqs. (2) dimensionless, we normalize distance by R, time by $\tau = \gamma R^2/K$ corresponding to the relaxation time scale of the nematic phase over the length scale of the droplet, and stress by the elastic stress $\sigma = K/R^2$. All the other quantities are rescaled accordingly. We have focused on the interplay between the surface tension Σ of the droplet and the contractile active stress $\alpha > 0$ and kept the other parameters constant ($\lambda = 0.1$, $\eta = M = 1$, $W = 1.25$, $\epsilon = \delta = 0.15$).

It is well known that, in bulk systems, contractile and extensile active stresses favor, respectively, splayed and bent configurations of the nematic director through feedback mechanisms mediated by the flow [33]. As a consequence, a uniformly oriented reference configuration becomes unstable once the internal active stress exceeds a critical value $\alpha_{\rm c} \sim \eta/\tau$ [11,21]. In nematic droplets, the director field is forced to have defects as a consequence of the disk topology and the normal orientation at the interface. This is achieved by forming two $+1/2$ disclinations approximately located at a distance of order $\epsilon = \delta\sqrt{W/K}$ from the droplet boundary, see Fig. 1(a) and Supplementary Material [34]. In passive nematic droplets, the defects repel each other with a force inversely proportional to their distance. This repulsion is in turn balanced by surface tension leading to a slight elongation of the droplet along the line joining the defects [25].

The scenario outlined above is dramatically altered by the presence of activity. Fueled by the strong distortion introduced by a defect, the active stresses give rise to a flow whose magnitude and direction is controlled by the activity constant α [35]. For a contractile droplet ($\alpha > 0$) with homeotropic boundary, the axisymmetric structure of the director drives a typical quadrupolar straining flow, causing

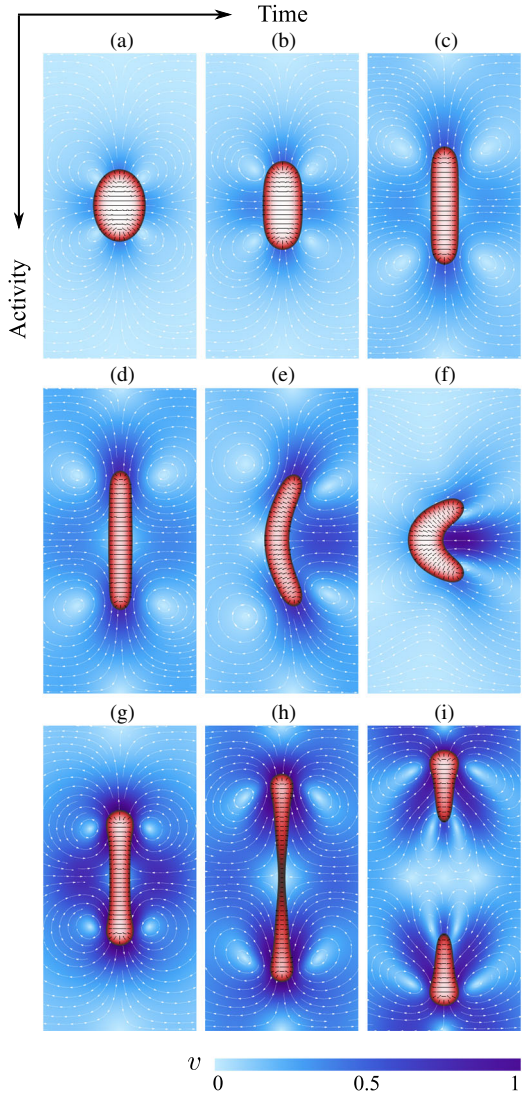

FIG. 1 (color online). The three behaviors of an active nematic droplet for fixed surface tension $\Sigma = 2.6$ and varying activity obtained from a numerical solution of Eq. (2). (a)–(c) For small activity the droplet stretches under the effect of the quadrupolar straining flow generated by the pair of $+1/2$ disclinations. (d)–(f) For $\alpha = 16$, the uniformly oriented director field in the interior of the droplet is unstable to splay and the droplet deforms. Following the deformation of the droplet, the backflow is no longer axially symmetric and this causes the droplet to move. (g)–(i) For very large activity ($\alpha = 36$), the capillary forces are no longer sufficient to balance the initial straining flow and the droplet divides. Movies displaying the time evolution of each state are included as Supplementary Material [34].

a much more drastic elongation than that produced by the elastic repulsion alone [Fig. 1(c)].

To characterize the spontaneous deformation we have measured the extension of the droplet as a function of the activity parameter α, for various Σ values [Fig. 2(a)]. This shows a clear linear behavior except for small α values, where the deformation is mainly dictated by the elastic repulsion between the defects. This behavior is consistent with the general picture of drop deformation in a straining flow [36,37]. According to this, a neutrally buoyant droplet placed in a shear flow experiences a strain that scales linearly with the capillary number $\mathrm{Ca} = \eta v/\Sigma$. Now, the velocity of the flow generated by an active nematic disclination scales like $v \sim \alpha R/\eta$ [35], hence, the linear dependence of the droplet extension on α. Moreover, by introducing an active variant of the capillary number, defined as $\mathrm{Ca}_\alpha = \alpha R/\Sigma$, one can rescale the numerical data and collapse them on the same master curve [Fig. 2(a), inset].

For larger activity the droplet becomes motile. Like in the case of active polar droplets [38,39], motility is achieved by means of a spontaneous splay deformation arising from the instability of the configuration of lowest nematic energy. As for static deformations, the droplet initially elongates as a consequence of the quadrupolar straining flow driven by the defects [Fig. 1(d)]. In the configuration of maximal elongation, the director field in the interior of the droplet is rather uniform, but after some time it starts to spontaneously splay [Fig. 1(e)]. The splayed configuration of the director field breaks the axial symmetry of the systems and transforms the quadrupolar flow

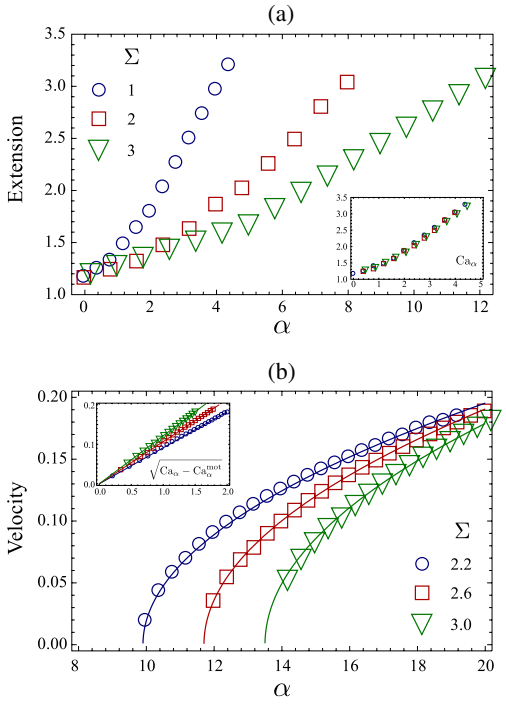

FIG. 2 (color online). (a) Extension of the droplet versus activity for various Σ values. The data collapse on the same master curve when rescaled with respect to the active capillary number $\mathrm{Ca}_\alpha = \alpha R/\Sigma$ (inset). (b) The velocity of a motile droplet versus activity for various Σ value. When rescaled with respect to Ca_α, the data intersect at the critical capillary number $\mathrm{Ca}_\alpha^{\mathrm{mot}} \approx 4.5$ (inset). The solid lines show the typical square-root law and are obtained from a fit.

in a dipolar flow consisting of two large vortices running across the droplet. This causes the droplet to move at constant velocity along its symmetry axis [Fig. 1(f)]. Figure 2(b) shows a plot of the center of mass velocity versus α for various Σ values; due to the initial axial symmetry, the onset of motion occurs as a supercritical bifurcation and the velocity follows a typical square-root scaling law [38]. Unlike the extension curve, the rescaled velocity data do not collapse on the same curve, but they do intersect at the critical point [Fig. 2(b), inset]. This implies that, while activity and surface tension independently affect the motion of active droplets, the onset of motility is controlled uniquely by the active capillary number Ca_α. With the choice of parameters used here the motility transition occurs at $\mathrm{Ca}_\alpha^{\mathrm{mot}} \approx 4.5$. The motility mechanism described here can be classified as a particular form of *swimming*: the droplet generates a flow in an ambient fluid and uses this to propel itself. In the presence of a substrate, several alternative motility mechanisms, which do not involve hydrodynamic flow and are collectively known as *crawling*, are possible [40–42].

Motility occurs as the combination of two processes: the initial elongation of the droplet, driven by the straining flow produced by the defects, and the instability of this configuration to splay. The existence of the intermediate elongated configuration is guaranteed by the fact that viscous and pressure forces exerted by the flow on the droplet are balanced by the resistance due to interfacial tension forces. For large capillary numbers, the capillary forces are no longer sufficient to achieve this balance, the droplet continuously stretches and eventually divides *before* the splay instability can develop [Figs. 1(g)–1(i)]. Our numerical data indicate that division occurs at a critical value $11.4 < \mathrm{Ca}_\alpha^{\mathrm{div}} < 16$. Once the parent droplet first divides, the active capillary number drops due to the reduction in the droplet size R. Thus, the two daughter droplets remain stable unless the activity is large enough that the new capillary number is itself larger than $\mathrm{Ca}_\alpha^{\mathrm{div}}$, in which case multiple divisions occur. This mechanism can, in principle, lead to a cascade of divisions that terminates only once the size of the youngest generation of droplets is such that $\mathrm{Ca} < \mathrm{Ca}_\alpha^{\mathrm{div}}$. Figure 3 shows a phase diagram in the (α, Σ) plane summarizing the three behaviors described so far.

The results presented here are strictly valid for a two-dimensional fluid. When including the effect of three dimensionality, several aspects of the droplet behavior remains, however, qualitatively unchanged. The active flow associated with axisymmetric droplets, for instance, has the structure illustrated in Fig. 1. Thus, both spontaneous stretching and division, which do not alter the axial symmetry of the droplet, would occur in three dimensions in the same way as described here. The splay deformation that determines the regime of motility does instead break axial symmetry. This, however, does not prevent motility from setting in three-dimensional systems as demonstrated in [38] for polar droplets. In the case of a thin film of active nematic suspended in a bulk Newtonian fluid, on the other hand, the frictional damping exerted by the surrounding fluid dissipates momentum through a force of the form $\boldsymbol{f}_{\mathrm{fri}} = -\xi \boldsymbol{v}$ in Eq. (2b). Such a frictional interaction removes energy from the flow at scales $\ell_{\mathrm{fri}} = \sqrt{\eta/\xi}$ and has no effect on the mechanics of the droplet as long as $\ell_{\mathrm{fri}} \gg R$.

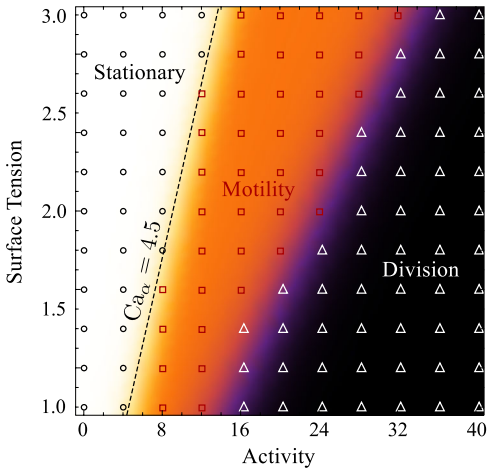

FIG. 3 (color online). Phase diagram showing the three classes of behavior exhibited by contractile active droplets for different α (activity) and Σ (surface tension). For low activity, the quadrupolar straining flow generated by the pair of $+1/2$ disclinations leads to a stationary elongated shape. When the activity is very strong, the active backflow causes the droplet to spontaneously divide. For intermediate activity and sufficiently large surface tension the director spontaneously splays and the droplet moves as a consequence of the associated backflow.

In conclusion, we have investigated the mechanics of a contractile active nematic droplet surrounded by a Newtonian fluid. Because of the interplay between the active stresses and the defective geometry of the nematic director, the system is able to mimic two of the defining functions of living cells: spontaneous division and motility, which can be selectively activated by controlling a single physical parameter: the active capillary number. Suspensions of microtuble bundles and kinesin, as those pioneered by Sanchez *et al.* [43], could serve as the backbone for an experimental realization of these nematic automata. In this case, however, the extensile active stresses (i.e., $\alpha < 0$) will have to be combined with tangential anchoring in order for the resulting active backflow to produce the same stretching mechanism described here. While bridging the gap between biological complexity and theoretical modeling remains a challenge for the future, our results provide a conceptual guidance to study the basic physical mechanisms behind motility and spontaneous division.

L. G. is grateful to Rastko Sknepnek and Luca Heltai for help with the simulations, and to Giovanni Romeo, whose unforgettable passion and curiosity have been inspirational throughout this work. A. D. S. acknowledges the ERC Advanced Grant No. 340685 MicroMotility.

[1] J. W. Szostak, D. P. Bartel, and P. L. Luisi, Nature (London) **409**, 387 (2001).
[2] C. A. Hutchison, S. N. Peterson, S. R. Gill, R. T. Cline, O. White, C. M. Fraser, H. O. Smith, and J. Craig Venter, Science **286**, 2165 (1999).
[3] S. Rasmussen, L. Chen, M. Nilsson, and S. Abe, Artif. Life **9**, 269 (2003).
[4] H. Fellermann, S. Rasmussen, H. J. Ziock, and R. V. Solé, Artif. Life **13**, 319 (2007).
[5] M. M. Hanczyc and J. W. Szostak, Curr. Opin. Cell Biol. **8**, 660 (2004).
[6] K. Takakura and T. Sugawara, Langmuir **20**, 3832 (2004).
[7] K. Kurihara, M. Tamura, K. Shohda, T. Toyota, K. Suzuki, and T. Sugawara, Nat. Chem. **3**, 775 (2011).
[8] P. L. Luisi and P. Stano, Nat. Chem. **3**, 755 (2011).
[9] M. M. Hanczyc, Phil. Trans. R. Soc. B **366**, 2885 (2011).
[10] K. Kruse, J. F. Joanny, F. Jülicher, J. Prost, and K. Sekimoto, Phys. Rev. Lett. **92**, 078101 (2004).
[11] L. Giomi, L. Mahadevan, B. Chakraborty, and M. F. Hagan, Phys. Rev. Lett. **106**, 218101 (2011).
[12] F. G. Woodhouse and R. E. Goldstein, Phys. Rev. Lett. **109**, 168105 (2012).
[13] M. G. Forest, Q. Wang, and R. Zhou, Soft Matter **9**, 5207 (2013).
[14] T. J. Pedley and J. O. Kessler, Annu. Rev. Fluid Mech. **24**, 313 (1992).
[15] H. Gruler, U. Dewald, and M. Eberhardt, Eur. Phys. J. B **11**, 187 (1999).
[16] H. Y. Lee and M. Kardar, Phys. Rev. E **64**, 056113 (2001).
[17] T. B. Liverpool and M. C. Marchetti, Phys. Rev. Lett. **90**, 138102 (2003).
[18] M. C. Marchetti, J. F. Joanny, S. Ramaswamy, T. B. Liverpool, J. Prost, M. Rao, and R. Aditi Simha, Rev. Mod. Phys. **85**, 1143 (2013).
[19] C. Martino, L. Horsfall, Y. Chen, M. Chanasakulniyom, D. Paterson, A. Brunet, S. Rosser, Y.-J. Yuan, and J. M. Cooper, Chem. Bio. Chem. **13**, 792 (2012).
[20] D. Marenduzzo, E. Orlandini, M. E. Cates, and J. M. Yeomans, Phys. Rev. E **76**, 031921 (2007).
[21] L. Giomi, L. Mahadevan, B. Chakraborty, and M. F. Hagan, Nonlinearity **25**, 2245 (2012).
[22] A. Baskaran and M. C. Marchetti, Phys. Rev. E **77**, 011920 (2008).
[23] A. W. C. Lau and T. C. Lubensky, Phys. Rev. E **80**, 011917 (2009).
[24] E. Bertin, H. Chaté, F. Ginelli, S. Mishra, A. Peshkov, and S. Ramaswamy, New J. Phys. **15**, 085032 (2013).
[25] P. Yue, J. J. Feng, C. Liu, and J. Shen, J. Fluid Mech. **515**, 293 (2004).
[26] L. Modica, Arch. Ration. Mech. Anal. **98**, 123 (1987).
[27] X. Yang, M. G. Forest, C. Liu, and J. Shen, J. Non-Newtonian Fluid Mech. **166**, 487 (2011).
[28] D. M. Anderson, G. B. McFadden, and A. A. Wheeler, Annu. Rev. Fluid Mech. **30**, 139 (1998).
[29] M. Brassel and E. Bretin, Math. Models Methods Appl. Sci. **34**, 1157 (2011).
[30] J. Rubinstein and P. Sternberg, IMA J. Appl. Math. **48** 249, (1992).
[31] P. G. de Gennes and J. Prost, *The Physics of Liquid Crystals* (Clarendon Press, Oxford, 1993).
[32] M. Nobili and G. Durand, Phys. Rev. A **46**, R6174 (1992).
[33] R. Voituriez, J. F. Joanny, and J. Prost, Europhys. Lett. **70**, 404 (2005).
[34] See Supplemental Material at http://link.aps.org/supplemental/10.1103/PhysRevLett.112.147802 for movies of droplet dynamics.
[35] L. Giomi, M. J. Bowick, X. Ma, and M. C. Marchetti, Phys. Rev. Lett. **110**, 228101 (2013).
[36] J. M. Rallison, Annu. Rev. Fluid Mech. **16**, 45 (1984).
[37] H. A. Stone, Annu. Rev. Fluid Mech. **26**, 65 (1994).
[38] E. Tjhung, D. Marenduzzo, and M. E. Cates, Proc. Natl. Acad. Sci. U.S.A. **109**, 12381 (2012).
[39] C. A. Whitfield, D. Marenduzzo, R. Voituriez, and R. J. Hawkins, Eur. Phys. J. E **37**, 8 (2014).
[40] H. Levine and W. Reynolds, Phys. Rev. Lett. **66**, 2400 (1991).
[41] F. Ziebert, S. Swaminathan, and I. S. Aranson, J. R. Soc. Interface **9**, 1084 (2012).
[42] F. Ziebert and I. S. Aranson, PLoS One **8**, e64511 (2013).
[43] T. Sanchez, D. N. Chen, S. J. DeCamp, M. Heymann, and Z. Dogic, Nature (London) **491**, 431 (2012).